Optimization of the hydrodynamic performance of a Vertical Axis Tidal (VAT) Turbine using CFD-Taguchi approach

Mohammad Hassan Khanjanpour, Akbar A. Javadi*

Department of Engineering, University of Exeter, Exeter, EX4 4QF, UK.

*Corresponding author

*Akbar A. Javadi

Tel: +44 1392 723640,

Email: A.A.Javadi@exeter.ac.uk

Abstract

Vertical Axis Tidal (VAT) turbines are used as ocean-powered devices to generate electricity from movements in ocean as a renewable source of energy. In this research, a number of CFD simulations have been carried out using the mixed-level modified Taguchi technique to determine the optimal hydrodynamic performance of a VAT turbine. The influence of four parameters: twist angle, camber position, maximum camber, and chord/radius ratio has been studied. The interaction of these parameters is investigated using the Variance of Analysis (ANOVA) approach. The Taguchi analysis showed that the most significant parameter affecting hydrodynamic performance of the turbine is the twist angle and the least effective parameter is chord/radius ratio. The ANOVA interaction analysis showed that the twist angle, camber position and maximum camber have significant interaction with each other. The results showed that the power coefficient (C_p) for the optimized VAT turbine is improved by 24% compared to the baseline design. Analysis of the pressure coefficient (Q_p) indicates that the hydrodynamic performance of VAT turbine is sensitive to cambered blade. Moreover, the flow separation in the optimized model is greatly reduced in comparison with the baseline model, signifying that the twisted and cambered blade could be effective in normalizing the spraying vortices over blades due to suppressing dynamic-stall. The findings of this research can provide guidelines for optimization of vertical turbines.

Keywords: VAT Turbine, Optimization, Taguchi method, ANOVA, Orthogonal Arrays, Hydrodynamic performance, CFD.

Nomenclature			
VAT	Vertical Axis Tidal	K	Quality loss factor
HAT	Horizontal Axis Tidal	V_t	Target quality
S/N	Signal to noise	V_e	Calculated response
H	Blade height (m)	n	number of the observed response
D	Length of blade chord (m)	Y	Observed response
r	Radius of turbine (m)	Y_m	Average of the observed response
α	Angle of attack (^{o})	σ	Solidity ratio
C_p	Power coefficient	N_b	Number of blades
P_o	Output power	η	Average of total mean S/N ratios

λ	Tip speed ratio	η^o	Estimated S/N ratio
C_t	Moment coefficient	η^*	Interaction term
T	Torque (N.m)	θ	Effect of each factor
ρ	Density of water (kg/m^3)	P	Pressure (Pa)
S	Blade area (m^2)	P_i	Freestream pressure (Pa)
U	Velocity of water (m/s)	Q_p	Pressure coefficient
ω	Angular velocity (rad/s)	S^2	Variance

1. Introduction

With the increasing interest and dependency on clean energies, the reliability and predictability of the energy resources become essential. One of the most reliable and predictable sources of renewable energy is tidal energy [1]. Tidal energy is estimated to have a global potential of 120 *GW* and could generate up to 150 *TWh* annually [2, 3]. Tidal turbines are used as sea-powered convertors to produce electricity or desalinate saline water [4, 5]. Similar to wind turbines, tidal turbines are divided into Vertical Axis Tidal (VAT) turbines and Horizontal Axis Tidal (HAT) turbines [6]. HAT turbines consist of a radial axis rotor which is parallel to the inlet water flow. With its drag or lift style blades, which are usually perpendicular to the rotational axis, it can convert the kinetic energy of water to mechanical energy [7]. On the other hand, in VAT turbines, the radial axis rotor is perpendicular to the inlet water flow and, similar to HAT turbines, their blades can be either drag or lift style [8]. VAT turbines have advantages of simple structure and independency to stream path in comparison to HAT turbines, and have been commonly used in both small and medium scales [9]. According to Kumar et al. [10], the number of published papers on optimization of tidal turbines is significantly less than wind turbines (see Figure 1). Table 1 presents a review of the notable optimization procedures conducted on VAT turbines in terms of optimization methods, objective functions, optimized parameters, and results. As it can be seen in this table, there are different parameters that need to be optimized for design, as well other parameters (e.g., roughness) that affect the performance of VAT turbines during their operation [11]. A review of research on turbines indicates that three parameters, namely twist angle [12], camber [13], and chord/radius ratio

[14] could have significant effect on turbine performance. The impacts of these three parameters on performance of VAT turbines have not been investigated in depth and their combined effects are unknown thus far. In this research, the effects of these three parameters on turbine performance are studied simultaneously. The Taguchi method is one of the powerful optimization methods in product design. The method, also known as the Robust Design method, significantly improves the performance and quality of engineering products [15]. The basic concept of the Taguchi theory is to improve a product's quality by minimizing the number of needed experiments without removing the parameters [16]. The Taguchi method offers Orthogonal Arrays (OA) or matrix of experiments (as a mathematical tool) in order to implement minimum experiments for providing wide range of variables to make better decision. For constructing OA, equal-level or mixed-level pattern can be used depending on the problem to be investigated. Mix-level Taguchi method provides a wider range of levels for significant factors [17]. Moreover, the Taguchi method introduces the signal to noise (S/N) ratio which can be used to calculate the quality of the output that is deviated from the desired values. In other words, the S/N ratio is an indicator for measuring the quality and also Orthogonal Arrays (OA) is to provide minimum design parameters concurrently [18]. The target quality of output is a key factor in the Taguchi method and should be defined for every application. The Taguchi method can be combined with numerical simulation (e.g., Computational Fluid Dynamic, CFD) models [19] in order to estimate optimized parameters. In this work, the objective is to maximize the performance of a tidal turbine. The power coefficient (C_p) which is an indicator of output, can be calculated from CFD simulations. Recently, the Taguchi technique has been used for optimizing turbine parameters. In 2015, Rao [20] optimized a Vertical Axis Wind (VAW) turbine by using the Taguchi method. In their work, the impacts of wake revolution and tip loss were considered when calculating the performance of the VAW turbine. They defined two different sets of parameters and levels,

called inner and outer loops, and analyzed each one separately. They used a standard L_{27} (3^{10}) OA for the inner loop and a standard L_{12} (2^9) OA for each outer loop. In the design phase, the performance of the turbine was maximized by focusing on blade size and twist angle as the design parameters. The results showed an increase of 52.7% in the efficiency of the turbine. Although they considered blade size, the effects of cambered airfoil was overlooked.

In 2018, Wang et al. [21] optimized the efficiency of VAW turbine by using CFD and Taguchi technique. They considered amplitude, wavelength, and twist angle as the design parameters and power coefficient (C_P) as the objective function. They used a standard L9 (3^4) OA for the Taguchi technique. Although, they improved the VAW turbine efficiency by 18% and provided valuable information about using the Taguchi technique for optimizing turbines, there was a significant gap in the selected levels for twist angle of blade, which has tremendous effect on the performance of turbine.

Permanasari et al. [22] used the Taguchi method to optimize a water wheel turbine in 2019. They considered flow rate, number of buckets, and blade size as design variables and a standard L_{16} (4^3) OA for the Taguchi method. The optimized parameters achieved 4% higher efficiency. In their work, the effects of hydrofoil (i.e., the cross section of a blade of tidal or water turbine which controls the hydrodynamic efficiency of a turbine for a specified flow environment) was not considered [23]. Review of the literature indicates that the impacts of combinations of twist angle, camber position, maximum camber, and chord/radius on performance of VAT turbines has not been studied. Moreover, the greatest weakness of these turbines is the high price of design and manufacturing. Traditionally, optimization of turbine efficiency is achieved by running several numerical models of the turbine which could become time consuming and expensive. In this work, an inexpensive method is developed and used to optimize a VAT turbine in order to maximize its hydrodynamic performance. The combined effects of twist angle, cambered blades, and solidity on performance of the VAT turbine is investigated. Using the mixed-level modified Taguchi approach and comprehensive 3D CFD simulations, a new set of optimized factors are identified and tested. The mean of the signal to noise (S/N) ratio is used to analyse how the selected factors affect the hydrodynamic performance of the VAT turbine, whilst ANOVA is used to evaluate the interaction of each factor with the others. Moreover, the physics of flow around the optimized and baseline turbines is evaluated and discussed.

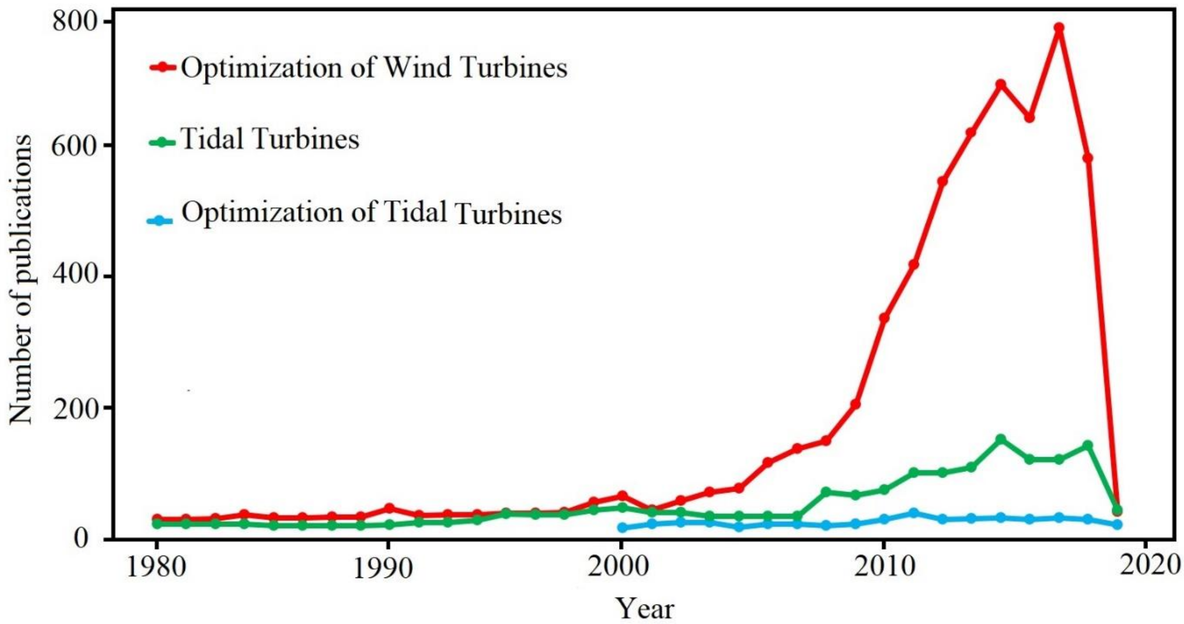

Figure 1. Publications on tidal turbines, optimization of tidal turbines, and optimization of wind turbines [10].

Table 1. Research works on VAT turbine optimization				
Researcher(s)	Method	Optimized parameters	Functional objectives	Results
Yong et al. [24]	Genetic algorithm	Chord/ Radius	Maximizing of the power coefficient	Optimizing the performance of VAT turbine about 20%
Alidadi [25]	Sequential Quadratic Programming	Duct	Maximizing of the power coefficient	Optimizing the performance of VAT turbine about 10%
Hwang et al. [26]	Genetic algorithm	Pitch angles	Maximizing of the power coefficient	Improving the performance of VAT turbine about 25%
Mannion et al. [27]	Blade element momentum theory	Solidity	Maximizing of the power coefficient	Improving the performance of VAT turbine about 10%
Luo et al. [28]	New mathematical strategy with regards to the rate of energy	Blade deflection angle	Maximizing of the power coefficient	Improving the performance of VAT turbine about 8%

2. Initial design, CFD modelling and validation

Initial design parameters of a VAT turbine are listed in Table 2. The blade height, chord length, and radius of the turbine are chosen as 0.4 m, 0.06 m, and 0.20 m respectively. In this section, the twist angle is zero and the blades are completely straight, and the number of turbine blades is three. For the hydrofoil, NACA 4-digit (XYZW) airfoils is chosen as they can be parameterized and also this type of airfoil has been used frequently in previous works for tidal turbines [29-32]. In this series, X is maximum camber, Y is camber position, and ZW is the value of thickness. Among the NACA 4-digit series airfoils [33] symmetric NACA0015 is selected. The basic terminology of an airfoil (or hydrofoil) is shown in Figure 2. The effect of a hydrofoil on the performance of the turbine depends on four parameters, chord length, blade thickness, camber position, and maximum camber.

Table 2. Initial parameters of VAT Turbine

Blade height (H)	0.4 m
Chord length (D)	0.06 m
Radius of the turbine (r)	0.2 m
Type of baseline hydrofoil	NACA 0015
Twist angle	0^{o}
Number of blades	3

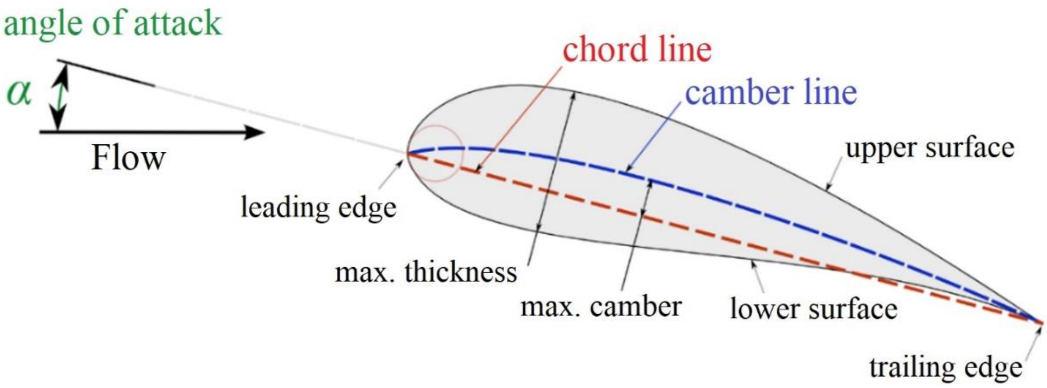

Figure 2. Basic hydrofoil terminology [34].

Figure 3 illustrates the general configuration of the straight-blade VAT turbine (baseline case) submerged in horizontal water flow. The inlet velocity is considered 1.0 m/s.

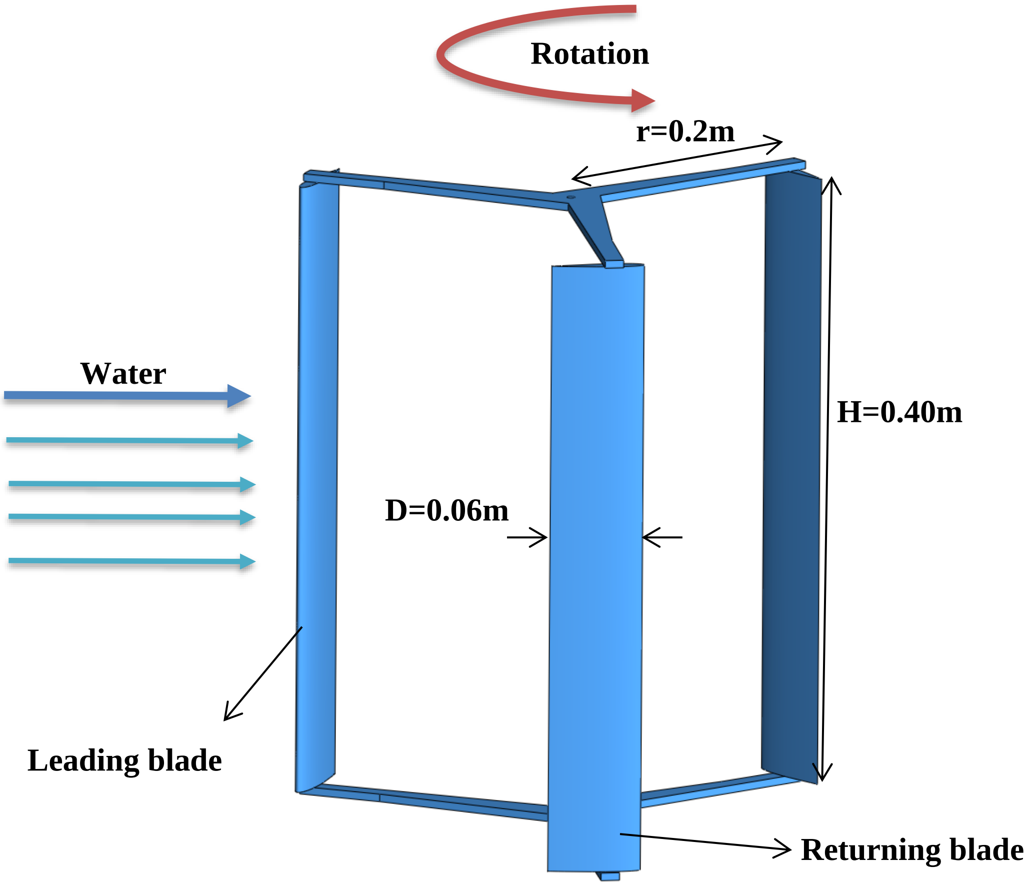

Figure 3. Schematic of the baseline VAT turbine.

Figure 4 summarises the computational domain and boundary conditions. Optimization of this domain is extremely important in order to decrease the time needed for computational runs and to provide sufficient space for suitable meshing. The computational domain is considered as a cubic domain of 1.5m*2.5m*7.0m for CFD modelling [35]. An unstructured mesh is built around the blades, whilst the rest of the domain is discretized using a structured mesh. A finer mesh is considered around the VAT turbine blade (Figure 5). A mesh sensitivity test is performed with 9 different grids for convergence analysis to find the optimal mesh size. The number of cells is increased consistently from 524,329 to 2,097,316, whilst the y+ (dimensionless wall distance) is 1 in all the tested grids. Considering that the torque of the turbine is not constant, the average output torque is used to measure the mean torque coefficient (C_t). The value of C_t for each of the 9 cases is determined using Eqs. 1 & 2 [36]. The results show that the relative standard deviation (RSD) of C_t for 1,048,658 cells is around 0.98 %. As in CFD analysis the computational cost increases rapidly with the number of cells, 1,048,658 cells is selected for the rest of the CFD simulations of the baseline model. A similar approach is used for all CFD tests in this paper.

A 3D transient and sliding mesh model is developed, using the ANSYS Fluent 19 software, for CFD analysis of the VAT turbine. The turbulence model of the Shear Stress Transport (SST) k-ω and the PISO (Pressure Implicit with Splitting of Operator) algorithm (coupling of the velocity and pressure equations) are adopted for the CFD simulation [37].

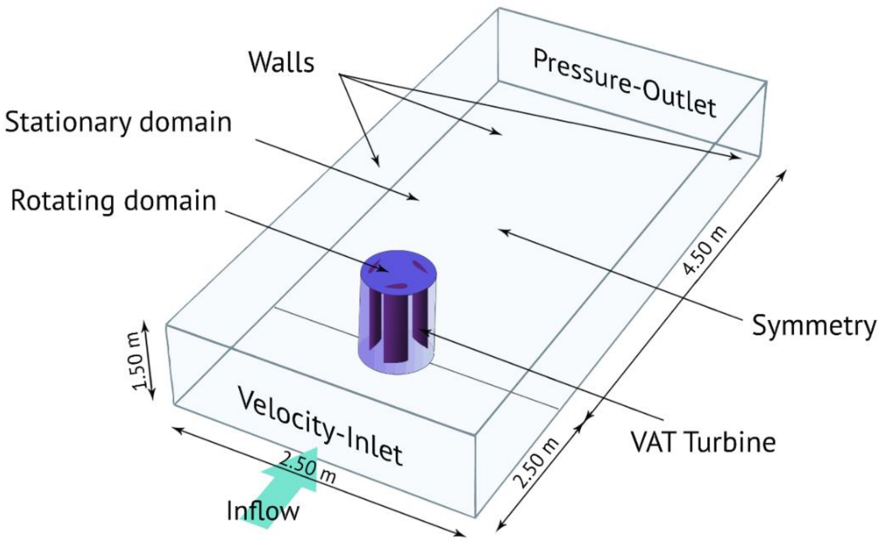

Figure 4. Computational domain and boundary conditions.

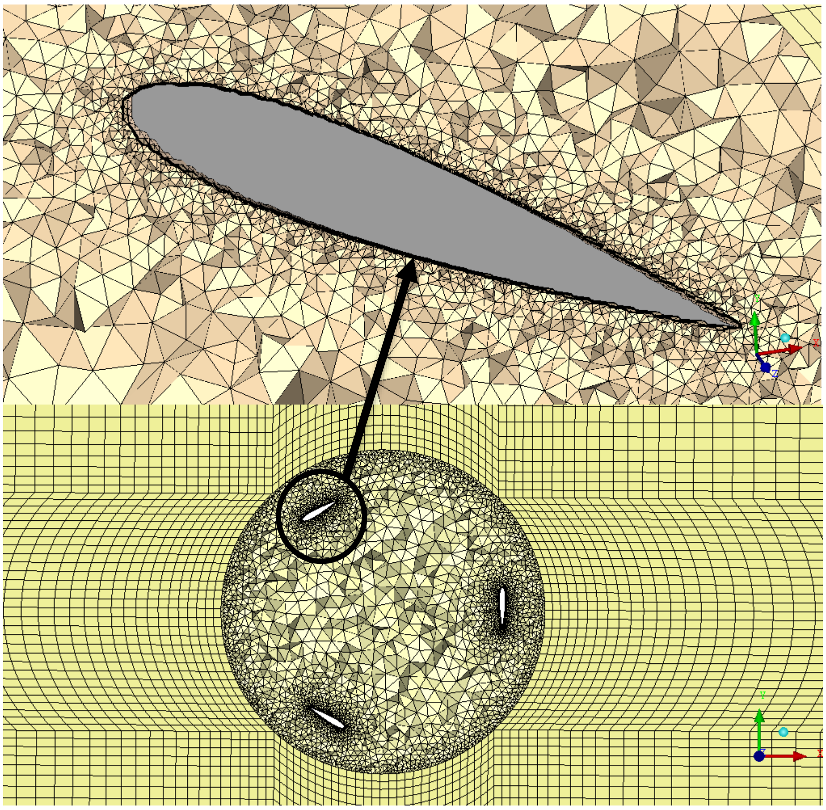

Figure 5. Intensive mesh around the blades.

One of the most common ways for validating CFD model for simulation of turbines is based on the power coefficient (C_p) (which is an indicator of the performance of turbines) and tip speed ratio (λ) (which is defined as the ratio of the water velocity to the velocity at the turbine blade tips) [38]. The baseline VAT turbine was fabricated by a 3D printer in the Engineering Department of the University of Exeter according to the selected dimensions (Table 2). An experimental model is developed to validate the CFD model. Figure 6 shows the fabricated turbine that is submerged in a large flume. For measuring the power coefficient (C_p) according to Eq. 3, the power output (P_o) of the baseline turbine is measured using an energy meter, a resistance panel, and a small electromotor. The energy meter's sensitivity for voltage and current is ±0.5%. Moreover, different tip speed ratios (λ) are provided by changing the water velocity based on Eq. 2. An Acoustic Doppler Velocimeter (ADV) is used to monitor the current stream patterns in the channel."

Figure 7 shows the variations of C_p with λ for both the numerical and experimental results, calculated using Eqs. 1-3 [39]. The power coefficient (C_p) of vertical turbines can be calculated by following equations:

$$C_t = \frac{T}{0.5\rho S U^3} \quad (1)$$

$$\lambda = \frac{\omega r}{U} \quad (2)$$

$$C_p = \frac{P_o}{0.5\rho S U^3} = \lambda C_t \quad (3)$$

where C_t: the moment coefficient, T: the torque; ρ: the density of water; S: the blade area; λ: the tip speed ratio, U: the velocity of water; ω: the angular velocity of turbine; r: the radius of turbine's hub; P_o: output power.

Figure 6. Experimental set up in a large flume at the Hydraulic Laboratory.

It can be seen from Figure 7 that, in general, the CFD results are in good agreement with the experimental results. However, there is some difference between CFD and experimental values. The main reason for this difference is that the CFD simulations assume rigid body geometries which overlook turbine blade hydroelastic behaviour [40, 41]. Vibration and deformation can adversely influence the performance of the turbines. In reality, the blades of the tidal turbine bend due to the pressure of the edge. The deformation of the turbine blades changes the angle of attack, which alters the pressure between the blade's low- and high-pressure sides. This results in reduction in turbine's output power. Accordingly, the difference between C_P values in the CFD and experimental analyses is less than 13% (with λ=1.25 which is used in all tests in this paper). However, the results indicate that this error is much greater at high tip speed ratios which can emphasize that the effects are higher at high speeds.

A review of previous research on turbines indicates that C_p : λ curves for all turbines have a peak point; i.e., the power coefficient increases with increasing λ up to a point beyond which, further increase in λ leads to reduction in C_p. For wind turbines, the maximum amount of power coefficient is limited to 16/27 (~0.59) according to the Betz Limit [42]. The maximum power coefficient of the baseline model is computed numerically as 0.16 at a tip speed ratio of 1.2.

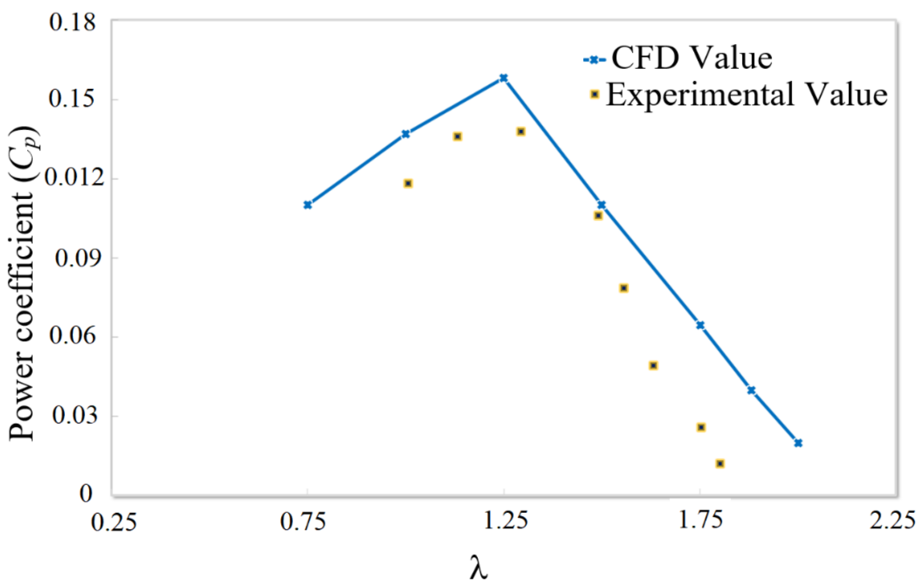

Figure 7. Comparison of CFD and experimental results for validation of the bassline case

3. Optimal design

3.1. Taguchi method

The Taguchi method provides an inexpensive and efficient way to find optimized geometry of devices by minimum number of experiments [43]. The process of identifying the optimal parameters can be summarized into seven steps [44]. The block diagram of the whole process is illustrated in Figure 8.

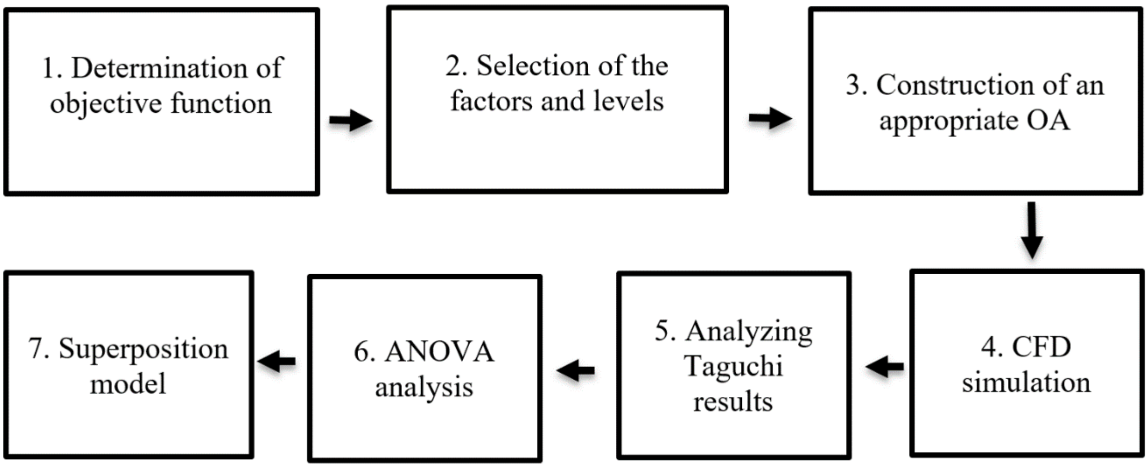

Figure 8. Block diagram of the process optimization.

Step 1: Determination of the objective function

To calculate the output of the VAT turbine and determine the objective function, a Quality Loss (QL) function (Eq. 4) is determined to measure a parameter's deviation from its target quality (the maximum amount that can be obtained) [45].

$$QL = K(V_e - V_t)^2 \tag{4}$$

where K: the quality loss factor; V_e: the calculated response; V_t: the target quality.

The QL function can estimate quality loss in a meaningful way [46]. In the current study, maximum power coefficient (C_p) is as the quality target. Vennell [47] states that the power coefficient of tidal turbines can exceed the C_p of wind turbines. Accordingly in this research, the maximum C_p is considered as 16/27 (corresponding to wind turbine) based on the Betz Limit which is a safe assumption [42].

The Taguchi method uses a signal to noise (S/N) ratio to measure the output volatility of the chosen variables as the optimization objective [48]. In the Taguchi technique, the S/N ratio for each category of products can be determined as follows [49]:

$$\text{Larger} - \text{the} - \text{better}: S/N_{LTB} = -10\, log \frac{1}{n} \sum_{i=1}^{n} \frac{1}{(Y_i)^2} \tag{5}$$

$$\text{Nominal} - \text{the} - \text{better}: S/N_{NTB} = 10\, log\, \frac{Y_m}{S^2} \tag{6}$$

$$\text{Smaller} - \text{the} - \text{better}: S/N_{STB} = -10\, log \frac{1}{n} \sum_{i=1}^{n} (Y_i)^2 \tag{7}$$

where Y: the observed response; Y_m: the mean of the observed responses; S^2: the variance; n: the number of the observed responses.

The Quality Loss function belongs to the “smaller – the – better” type problem class. In this study “small” refers to “QL function”. The QL function can generally be converted into an S/N ratio (Eq. 8) to measure the quality of a product [45].

$$S/N_{STB} = -10\, log(V_e - V_t)^2 \tag{8}$$

As it can be seen from Eq. 8, the margin between maximum and optimum responses must be as small as possible for maximising the S/N ratio. Maximizing V_e is equivalent to minimising quality loss in Eq. 8 which makes the noise sensitivity minimum [50]. Therefore, by replacing maximum power coefficient and target quality, the objective function can be defined as:

$$S/N = -10\, log\left(C_p - {}^{16}/_{27}\right)^2 \tag{9}$$

Step 2: Selection of the factors and levels

According to the parameter design tests, an optimal set of parameter response is defined as one that produces an inexpensive design while maintaining sufficient quality variation.

Determining the optimal amount of each factor can be achieved by choosing the factor levels with the maximum S/N ratio. In the Taguchi method, the goal is to find the optimum combination of controlling factors. In this study, four standard factors which have significant effects on the hydrodynamic performance of vertical turbines [51-56] are chosen, including twist angle (A), camber position (B), maximum camber (C), and chord/radius ratio (D).

The twist angle aims to minimize flow separation, making a positive lift at zero angle of attack (α) to allow self-start in ideal wind or water conditions. It also improves the performance of the turbine by increasing the blade's effective area [57]. As the selected VAT turbine has three blades, the total twist angle of experiments can be increased up to 120°. 6 levels have been selected for the twist angle, including, 20º, 40º, 60º, 80º, 100º, 120º.

The camber position in the NACA family of airfoils can be varied from 0% to 90%. For investigating this factor, 70%, 45%, and 20% have been selected as levels of camber position (B). Moreover, the maximum camber in NACA airfoils can vary from 0 to 9.5%. There levels of 2.5%, 5.0%, and 7.5% are chosen for this factor. In the current study the thickness of hydrofoil is considered as constant.

Solidity ratio is among the most important factors that influence the efficiency of vertical tidal turbines [58]. Solidity ratio is defined as the ratio of the swept area to total blade area of turbine [59]. As the highest power coefficient (C_p) can be dependent on solidity ratio [60], this ratio is chosen to be optimized.

The solidity ratio can be determined as [61]:

$$\sigma = \frac{N_b D}{2r} \tag{10}$$

where σ: the solidity ratio; N_b: the number of blades; D: the length of blade chord; r: the radius of turbine.

Since the number of the blades of the turbine is considered as three, a chord/radius ratio is considered to be optimized as a representative of the solidity ratio. Because, the solidity should not exceed 0.5 as the proximity of the blades degrades the turbine output [62], chord/radius ratios of 0.1, 0.2, and 0.3 are selected for this factor. All the above mentioned factors and their levels are summarized in Table 3.

Table 3. Determined factors and levels

Levels	1	2	3	4	5	6
A: Twist angle	20^0	40^0	60^0	80^0	100^0	120^0
Levels	1		2		3	
B: Camber position	0.70		0.45		0.20	
C: Maximum camber	0.025		0.050		0.075	
D: Chord/radius	0.10		0.20		0.30	

Step 3: Construction of an appropriate Orthogonal Array (OA)

In the Taguchi approach, only a certain number of experiments is needed to test according to the orthogonal array (OA) rather than all feasible models. Generally, the selected optimization approach needs a parameter matrix with a variety of levels that the parametric differences can be analyzed. The minimum number of tests that is required in the Taguchi method can be determined based on degrees of freedom (DOF) [63]. The OA is adjusted in the experimental design to test one factor at 6 levels and 3 factors at 3 levels. The possible OA for the total number of selected parameters and levels is L_{18} (6^1*3^3) (mixed-level orthogonal array) which is constructed as shown in Table 4. Accordingly, based on the constructed orthogonal array, instead of 162 cases, 18 cases will be analysed to achieve maximum hydrodynamic performance of the turbine determined by the four factors, namely twist angle (6 levels), camber position (3 levels), maximum camber (3 levels), and chord/ radius ratio (3 levels).

Table 4. L_{18} (6^1*3^3) Orthogonal array (OA)

No.	A	B	C	D
Run 1	1	1	1	1
Run 2	1	2	2	2
Run 3	1	3	3	3
Run 4	2	1	1	2
Run 5	2	2	2	3
Run 6	2	3	3	1
Run 7	3	1	2	1
Run 8	3	2	3	2
Run 9	3	3	1	3
Run 10	4	1	3	3
Run 11	4	2	1	1
Run 12	4	3	2	2
Run 13	5	1	2	3
Run 14	5	2	3	1
Run 15	5	3	1	2
Run 16	6	1	3	2
Run 17	6	2	1	3
Run 18	6	3	2	1

Step 4: CFD simulation

In this section, 18 different models (see Figure 9), according to the dimensions listed in Table 3 and the constructed OA (Table 4), are designed using SOLIDWORKS 2017 and simulated by ANSYS Fluent 2019 software in order to quantify the hydrodynamic performance of the turbines. The moment coefficients (C_t) for a single revolution at λ=1.25 for the baseline case and other 18 cases are calculated using Eq. 1 and the results are presented in Figure 10. Moreover, the power coefficients (C_p) are calculated using Eq. 3 and the results are presented in Table 5. From the results, it can be seen that the twist angle has an important effect on the output of the VAT turbine. The highest average moment coefficient (C_t) and power coefficient (C_p) correspond to case 12 which are 0.134 and 0.202 respectively. The value of C_p (0.202) obtained for case 12 is 21% higher than the C_p (0.16) for the baseline case which was calculated in section 2.

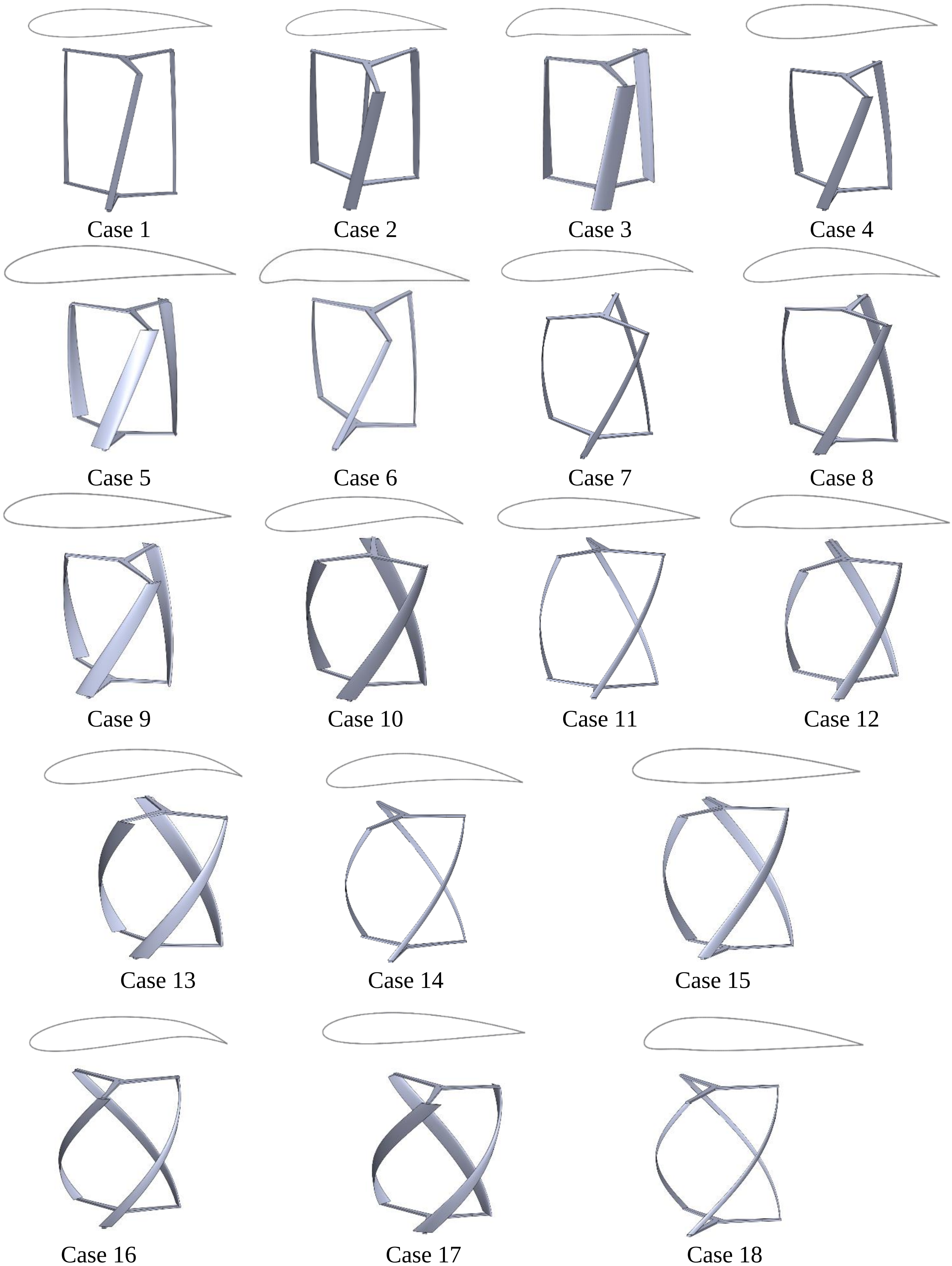

Figure 9. All turbine designs according to the L_{18} Orthogonal array (OA).

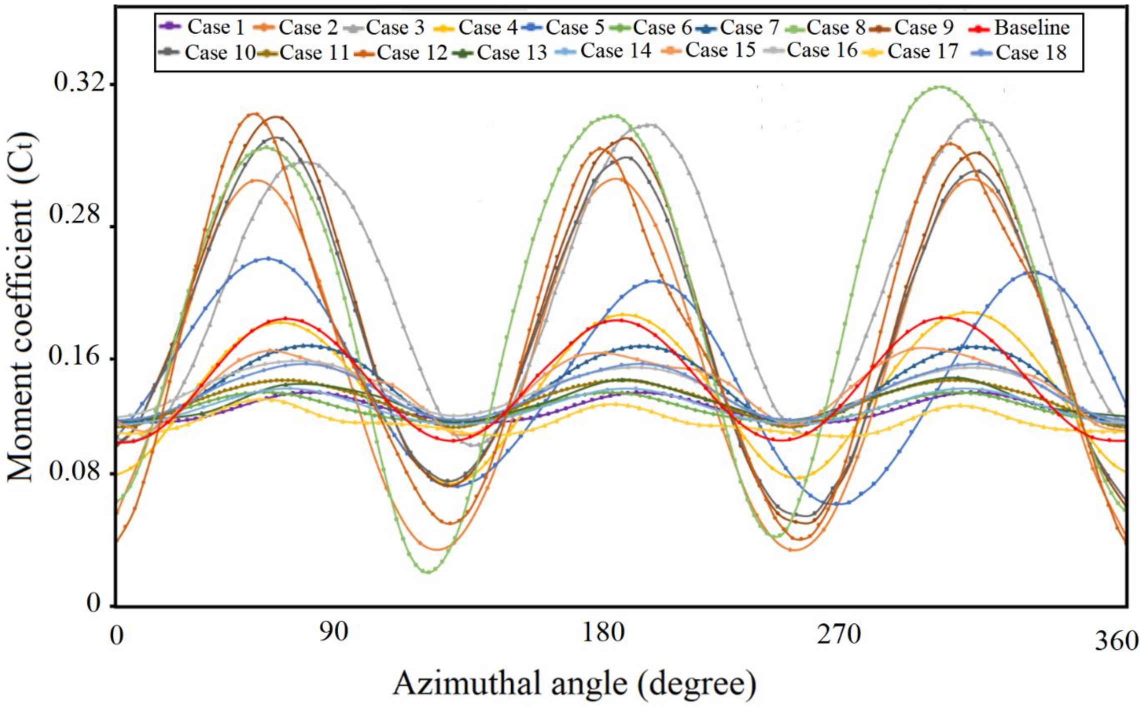

Figure 10. Variations in moment coefficient for single revolution, form 0° to 360° at water velocity of 1.0 m/s and λ=1.25.

Step 5: Analyzing Taguchi results

The S/N ratios of 18 different cases are calculated using Eq. 9 and the results are presented in Table 5. According to Eq. 9, the maximum S/N ratio occurs at the maximum power coefficient. The maximum S/N ratio is 8.232 which corresponds to case 12. In the next step, the Taguchi method is used to determine the order of impact and the optimal combination of the parameters to be selected for the design. The mean S/N ratios for parametric design are calculated using Eq. 9 and Table 5. For instance, the mean S/N ratio of A_6 is calculated from the average values of three level 6 factors $[(7.001 + 6.238 + 6.714)/3 = 6.651]$. Similarly, the S/N ratios are calculated for the rest of the factors with deferent levels and the results are plotted in Figure 11. The results show that the combination of A_4, B_3, C_2, and D_2 results in the maximum output. To find the order of the effect of each factor, a parameter (θ) is defined, which is the difference between the maximum and minimum responses of each factor. The values of this parameter for factors A, B, C, and D are 0.863, 0.136, 0.151, and 0.684 respectively. This implies that factor A, which is twist angle, is the most significant factor among the 4 tested factors, affecting the hydrodynamic performance of the turbine. Moreover, factors B (camber position) and C (maximum camber) have the least impact on the output power of the turbine.

Table 5. L_{18} Orthogonal array (OA)

No.	Twist angle	Camber position	Maximum camber	Chord/ Radius	C_p	S/N
Run 1	20°	0.70	0.025	0.10	0.148	7.099
Run 2	20°	0.45	0.050	0.20	0.169	7.522
Run 3	20°	0.20	0.075	0.30	0.160	7.338
Run 4	40°	0.70	0.025	0.20	0.172	7.584
Run 5	40°	0.45	0.050	0.30	0.143	7.001
Run 6	40°	0.20	0.075	0.10	0.148	7.099
Run 7	60°	0.70	0.050	0.10	0.147	7.079
Run 8	60°	0.45	0.075	0.20	0.192	8.011
Run 9	60°	0.20	0.025	0.30	0.155	7.238
Run 10	80°	0.70	0.075	0.30	0.132	6.790
Run 11	80°	0.45	0.025	0.10	0.169	7.522
Run 12	80°	0.20	0.050	0.20	0.202	8.232
Run 13	100°	0.70	0.050	0.30	0.142	6.982
Run 14	100°	0.45	0.075	0.10	0.146	7.060
Run 15	100°	0.20	0.025	0.20	0.140	6.943
Run 16	120°	0.70	0.075	0.20	0.143	7.001
Run 17	120°	0.45	0.025	0.30	0.102	6.238
Run 18	120°	0.20	0.050	0.10	0.128	6.714
Baseline	0°	N/A	N/A	0.30	0.159	N/A

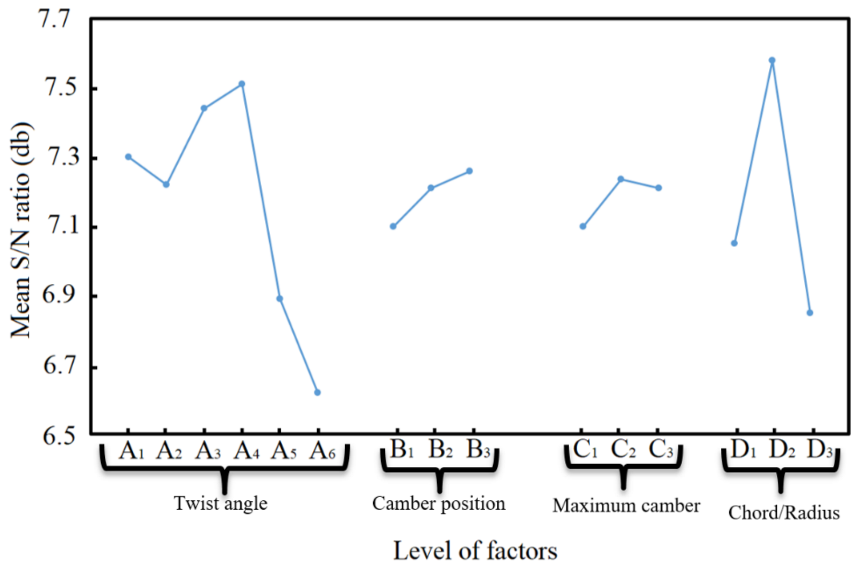

Figure 11. The mean S/N ratio for parametric design.

Step 6: Assessing the interactions between turbine parameters

Interactions between the turbine parameters are crucial and they should be considered in order to make the experiments and their analysis meaningful [21]. To evaluate the interaction of the turbine parameters, the two-way Analysis of Variance (ANOVA) technique is used for the S/N ratios. The ANOVA technique can be used to provide a measure of reliability. Instead of analysing the data directly, this method determines the data variability and analyses the mean difference in quality of experiments conducted [64, 65]. ANOVA interaction plot can be used to visualize the relationship between the factors [66, 67]. Figure 12 illustrates three different possible scenarios comprising two three-level factors according to the tested responses. In parallel trends, either interaction does not occur or is negligible while in non-parallel ones, the interaction between factors occurs and it must be considered [68]. In this analysis, the interaction of each two factors is calculated according to the S/N ratios listed in Table 5 and plotted in Figure 13. The mean S/N ratio interaction graphs illustrate that the major impacts on the responses is due to the interaction of twist angle (A) with other factors. The parallel patterns in the lines of interaction between D and other factors clearly indicate negligible interaction and therefore in the following section A*D, B*D, and C*D will not be applied.

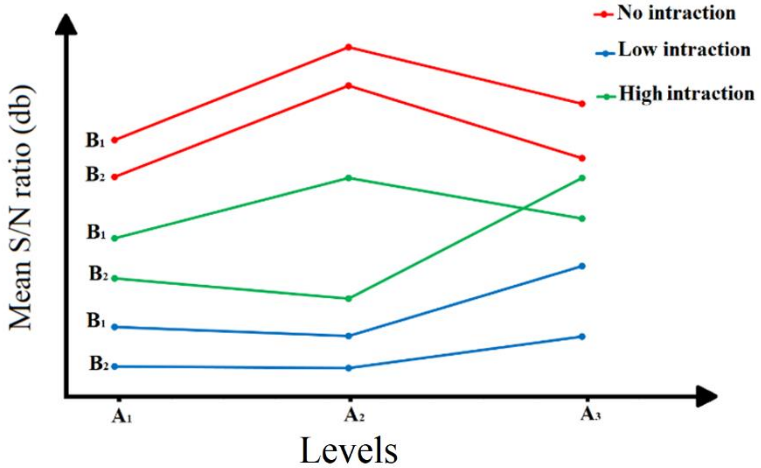

Figure 12. Interaction plot in three different possible scenarios.

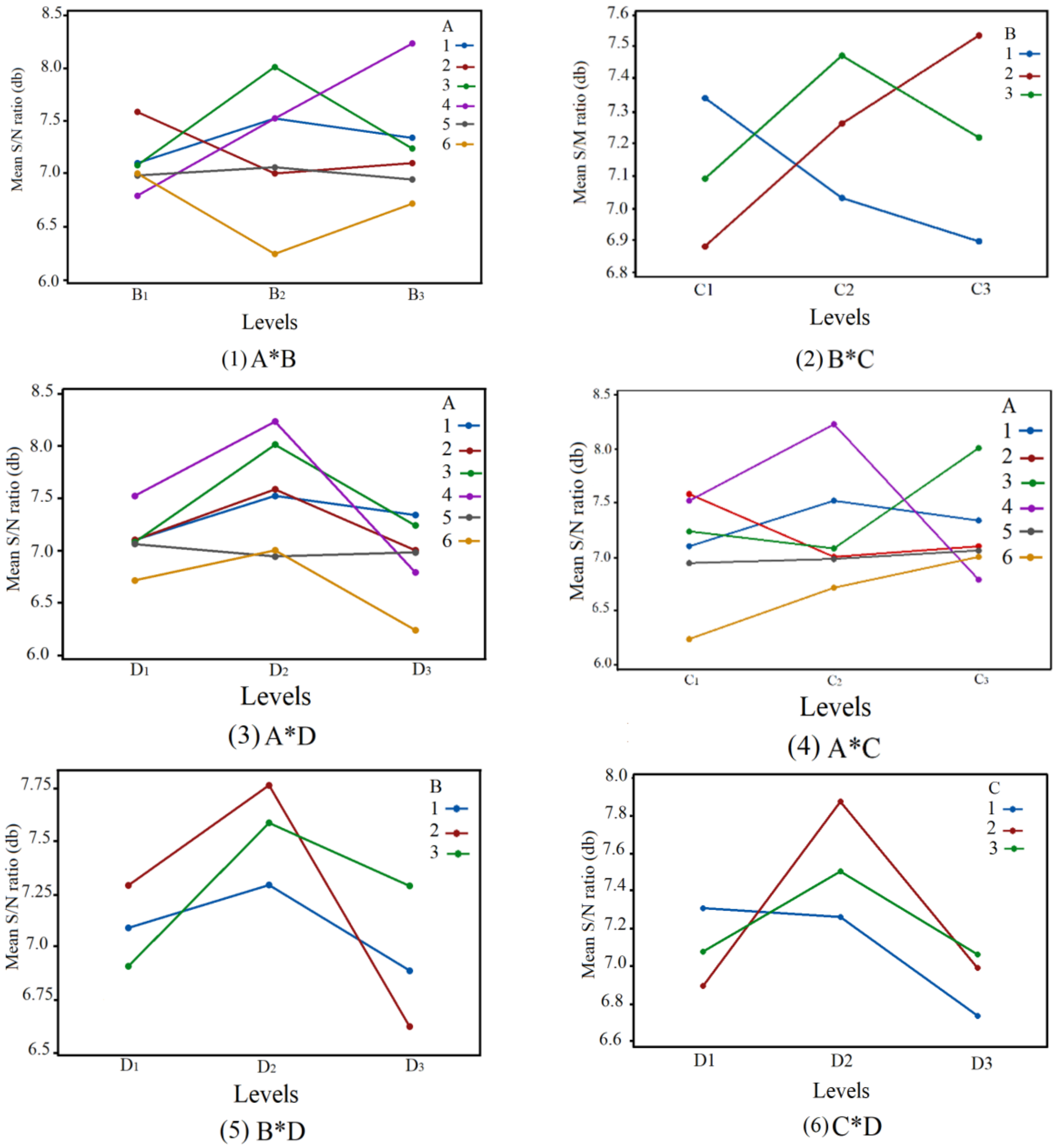

Figure 13. Interaction plot (ANOVA).

Step 7: Superposition model, considering the effects of interaction

Superposition model can be used to estimate all possible responses (S/N ratios) outside of orthogonal array (OA). According to Phadke [45], superposition model for the four factors, assuming that the amount of error is negligible, can be defines as:

$$\eta^{o}\left(A_i, B_j, C_k, D_l\right) = \eta + (\eta_{Ai} - \eta) + \left(\eta_{Bj} - \eta\right) + (\eta_{Ck} - \eta) + (\eta_{Dl} - \eta) \quad (11)$$

where η^{o}: the estimated S/N ratio; η: the average of total mean S/N ratios; $\eta_{Ai}, \eta_{Bj}, \eta_{Ck}, \eta_{Dl}$: the S/N ratios with the factors A, B, C, and D at levels i, j, k, and l respectively.

The superposition equation should be updated to contain the interaction of factors by adding extra terms in order to provide the impacts of relationship between any two variables. Accordingly, additional term of A and B is determined as follows:

$$\eta^{*}(A_i, B_j) = (\eta_{AiBj} - \eta) - (\eta_{Ai} - \eta) - (\eta_{Bj} - \eta) \qquad (12)$$

where η^{*}: the interaction term; η_{AiBj}: the average of total mean S/N ratios including both A_i and B_j.

This approach can be used for other interactions (A*B, A*C, and B*C) and by adding the interaction terms to the superposition equation, the modified superposition equation for calculating 162 (6*3*3*3) possible cases can be written as follows:

$$\eta^{t}(A_i, B_j, C_k, C_l) = \eta + (\eta_{Ai} - \eta) + (\eta_{Bj} - \eta) + (\eta_{Ck} - \eta) + (\eta_{Dl} - \eta) + (\eta_{AiBj} - \eta) - (\eta_{Ai} - \eta) - (\eta_{Bj} - \eta) + (\eta_{Aick} - \eta) - (\eta_{Ai} - \eta) - (\eta_{Ck} - \eta) + (\eta_{CkBj} - \eta) - (\eta_{Ck} - \eta) - (\eta_{Bj} - \eta) = -(\eta_{Ai}) - (\eta_{Bj}) - (\eta_{Ck}) + (\eta_{Dl}) + (\eta_{AiBj}) + (\eta_{AiCk}) + (\eta_{CkBj}) \qquad (13)$$

To solve Eq. 13, a program is written in MATLAB and by using the data in Table 5, the total possible S/N ratios for 162 cases are calculated and the results are presented in Table 6.

The results in Table 6 show that, the case 104 provides the maximum signal to noise ratio (9.456) in the combination of A_4, B_3, C_2, and D_2 that is considerably greater than the optimal case (case 12) with the combination of A_4, B_3, C_3, and D_2, calculated by 18 cases in the Taguchi orthogonal array.

Table 6. Estimated S/N ratios for all possible combinations

No.	A	B	C	D	Estimated S/N ratio	**No.**	A	B	C	D	Estimated S/N ratio	**No.**	A	B	C	D	Estimated S/N ratio
1	1	1	1	1	7.123	**55**	3	1	1	1	7.119	**109**	5	1	1	1	7.174
2	1	1	1	2	7.576	**56**	3	1	1	2	7.572	**110**	5	1	1	2	7.628
3	1	1	1	3	6.958	**57**	3	1	1	3	6.955	**111**	5	1	1	3	7.01
4	1	1	2	1	7.084	**58**	3	1	2	1	6.498	**112**	5	1	2	1	6.751
5	1	1	2	2	7.537	**59**	3	1	2	2	6.952	**113**	5	1	2	2	7.204
6	1	1	2	3	6.919	**60**	3	1	2	3	6.334	**114**	5	1	2	3	6.587
7	1	1	3	1	6.803	**61**	3	1	3	1	7.333	**115**	5	1	3	1	6.733
8	1	1	3	2	7.257	**62**	3	1	3	2	7.787	**116**	5	1	3	2	7.186
9	1	1	3	3	6.639	**63**	3	1	3	3	7.169	**117**	5	1	3	3	6.568
10	1	2	1	1	6.948	**64**	3	2	1	1	7.452	**118**	5	2	1	1	6.655
11	1	2	1	2	7.401	**65**	3	2	1	2	7.906	**119**	5	2	1	2	7.108
12	1	2	1	3	6.784	**66**	3	2	1	3	7.288	**120**	5	2	1	3	6.49
13	1	2	2	1	7.602	**67**	3	2	2	1	7.524	**121**	5	2	2	1	6.924
14	1	2	2	2	8.055	**68**	3	2	2	2	7.978	**122**	5	2	2	2	7.377
15	1	2	2	3	7.437	**69**	3	2	2	3	7.36	**123**	5	2	2	3	6.759
16	1	2	3	1	7.73	**70**	3	2	3	1	8.768	**124**	5	2	3	1	7.314
17	1	2	3	2	8.183	**71**	3	2	3	2	9.221	**125**	5	2	3	2	7.767
18	1	2	3	3	7.565	**72**	3	2	3	3	8.604	**126**	5	2	3	3	7.149
19	1	3	1	1	6.939	**73**	3	3	1	1	6.855	**127**	5	3	1	1	6.713
20	1	3	1	2	7.392	**74**	3	3	1	2	7.308	**128**	5	3	1	2	7.166
21	1	3	1	3	6.775	**75**	3	3	1	3	6.69	**129**	5	3	1	3	6.549
22	1	3	2	1	7.594	**76**	3	3	2	1	6.928	**130**	5	3	2	1	6.983
23	1	3	2	2	8.047	**77**	3	3	2	2	7.381	**131**	5	3	2	2	7.437
24	1	3	2	3	7.43	**78**	3	3	2	3	6.764	**132**	5	3	2	3	6.819
25	1	3	3	1	7.194	**79**	3	3	3	1	7.643	**133**	5	3	3	1	6.846
26	1	3	3	2	7.648	**80**	3	3	3	2	8.097	**134**	5	3	3	2	7.299
27	1	3	3	3	7.03	**81**	3	3	3	3	7.479	**135**	5	3	3	3	6.681
28	2	1	1	1	8.185	**82**	4	1	1	1	7.042	**136**	6	1	1	1	6.833
29	2	1	1	2	8.638	**83**	4	1	1	2	7.495	**137**	6	1	1	2	7.286
30	2	1	1	3	8.021	**84**	4	1	1	3	6.877	**138**	6	1	1	3	6.668
31	2	1	2	1	7.14	**85**	4	1	2	1	7.289	**139**	6	1	2	1	6.847
32	2	1	2	2	7.593	**86**	4	1	2	2	7.743	**140**	6	1	2	2	7.3
33	2	1	2	3	6.975	**87**	4	1	2	3	7.125	**141**	6	1	2	3	6.682
34	2	1	3	1	7.141	**88**	4	1	3	1	5.751	**142**	6	1	3	1	7.037
35	2	1	3	2	7.594	**89**	4	1	3	2	6.204	**143**	6	1	3	2	7.49
36	2	1	3	3	6.977	**90**	4	1	3	3	5.587	**144**	6	1	3	3	6.873
37	2	2	1	1	7.004	**91**	4	2	1	1	7.176	**145**	6	2	1	1	5.472
38	2	2	1	2	7.457	**92**	4	2	1	2	7.63	**146**	6	2	1	2	5.925
39	2	2	1	3	6.84	**93**	4	2	1	3	7.012	**147**	6	2	1	3	5.307
40	2	2	2	1	6.651	**94**	4	2	2	1	8.116	**148**	6	2	2	1	6.178
41	2	2	2	2	7.105	**95**	4	2	2	2	8.57	**149**	6	2	2	2	6.632
42	2	2	2	3	6.487	**96**	4	2	2	3	7.952	**150**	6	2	2	3	6.014
43	2	2	3	1	7.061	**97**	4	2	3	1	6.987	**151**	6	2	3	1	6.777
44	2	2	3	2	7.515	**98**	4	2	3	2	7.44	**152**	6	2	3	2	7.231
45	2	2	3	3	6.897	**99**	4	2	3	3	6.822	**153**	6	2	3	3	6.613
46	2	3	1	1	7.277	**100**	4	3	1	1	8.061	**154**	6	3	1	1	6.123
47	2	3	1	2	7.73	**101**	4	3	1	2	8.515	**155**	6	3	1	2	6.576
48	2	3	1	3	7.113	**102**	4	3	1	3	7.897	**156**	6	3	1	3	5.959
49	2	3	2	1	6.925	**103**	4	3	2	1	9.003	**157**	6	3	2	1	6.831
50	2	3	2	2	7.379	**104**	4	3	2	2	**9.456**	**158**	6	3	2	2	7.284
51	2	3	2	3	6.761	**105**	4	3	2	3	8.838	**159**	6	3	2	3	6.666
52	2	3	3	1	6.807	**106**	4	3	3	1	7.345	**160**	6	3	3	1	6.902
53	2	3	3	2	7.261	**107**	4	3	3	2	7.798	**161**	6	3	3	2	7.355
54	2	3	3	3	6.643	**108**	4	3	3	3	7.18	**162**	6	3	3	3	6.737

4. Fluid physics of the baseline and optimized VAT turbines

A new turbine is designed based on the obtained optimized dimensions in the previous section. Figure 13 shows a comparison of the new design and the baseline case design. The new design is simulated numerically, as described in section 2, and by using Eq. 3 and the data obtained from the CFD model, the power coefficient (*Cp*) is calculated as 0.210, which is 24% higher than the baseline case. Moreover, the optimized model reduces the required material by 57% compared with the baseline model, indicating that the new model is more economical.

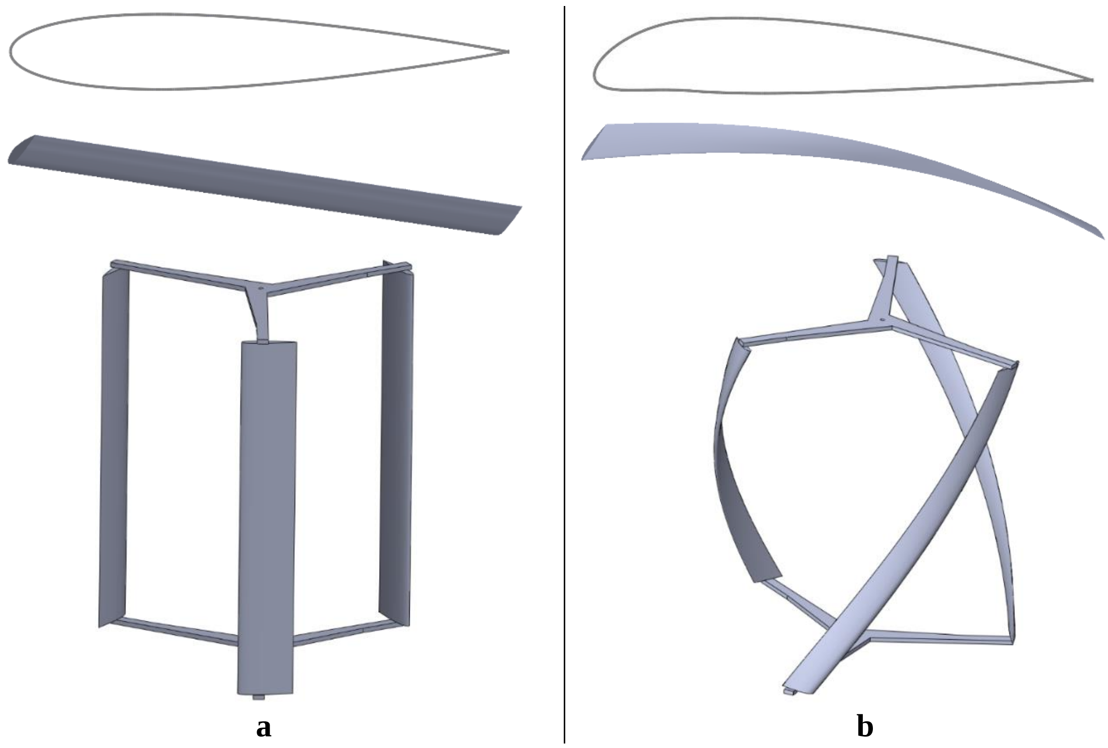

Figure 14. (a) Baseline and (b) optimized configurations.

Although the updated superposition in the Taguchi approach enables to determine the optimal configuration of the VAT turbine to gain a significant increase in hydrodynamic output, the fundamental fluid dynamics of this development still remains unknown. The pressure coefficient (Q_p) and the moment coefficient (C_t) around a single blade (leading blade) are calculated using the CFD data and the results show that the optimized turbine produces a promising improvement in power output.

The variations of moment coefficient (C_t) with azimuthal angle for the baseline and optimized models at λ= 1.25 are calculated and the results are presented in Figure 15. The results show that in the first half rotation, a significant part of positive moment contributions is located in the region between 40 ° and 180° and this is a very general characteristic demonstrated in several previous research [69, 70]. Although the maximum (C_t) in some parts of the graph (40-100°) of the baseline model is higher than that in the optimized model, however the combination of the cambered-blade and twisted model has advantages when the whole region is considered.

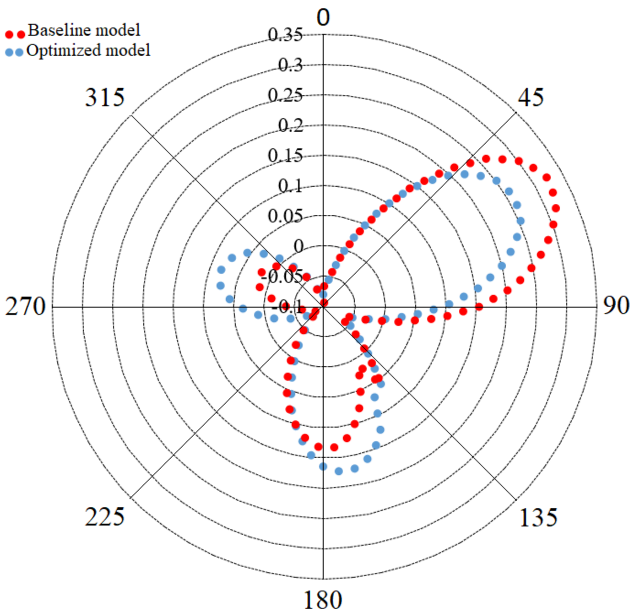

Figure 15. Moment coefficient (C_t) versus azimuthal angle (0-360 degree) for a single blade of the baseline and optimized models at λ = 1.25.

Since the efficiency of a VAT turbine is quite sensitive to the particular shape used for the hydrofoil [71], a qualitative assessment for the pressure coefficient for the baseline (symmetric) and cambered hydrofoils is performed to obtain a deeper understanding of this impact. The pressure coefficient over a hydrofoil can be determined by the pressure and stream properties as follows [72]:

$$Q_p = \frac{P - P_i}{0.5\rho S U^2} \quad (14)$$

where Q_p: the pressure coefficient; P: the pressure; P_i: the freestream pressure.

Figure 16 demonstrates the distribution of the pressure coefficient (Q_p) over leading blade for the baseline and optimized models at λ = 1.25 with the corresponding length of the chord. Q_p is negative at the bottom (lower surface) of hydrofoil and positive on its top (upper surface), and the hydrofoil's lift is heading upward. The suction peak is described as the highest suction value across the airfoil's bottom surface [73]. The suction peak of Q_p for the cambered hydrofoil is greater than the baseline hydrofoil. Moreover, the margin (the difference between suction and pressure levels) of Q_p at the cambered hydrofoil is much greater than the symmetric hydrofoil, indicating a greater lifting force in the cambered hydrofoil.

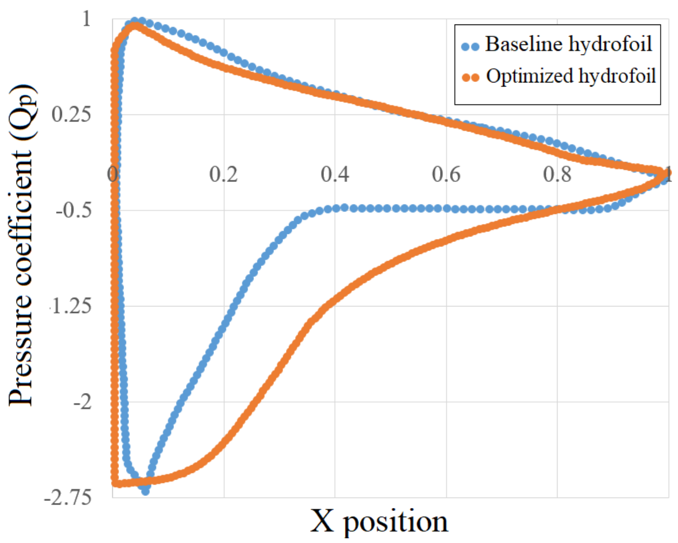

Figure 16. Pressure coefficient (Q_p) distribution for baseline and optimized hydrofoils at azimuthal angle: 45°.

One of the fluid dynamics phenomena which can be used to compare and analyse the baseline and optimized turbines is dynamic-stall. To visualize the flow around the turbine, vorticity contours at 4 azimuthal angles and 3 planes (I, II, and III) are plotted using CFD-Post ANYS 2019 (Figure 17). To analyse the performance of the turbine, a blade is indicated as IB (see

Figure 17) so that azimuthal angle could be measured. The azimuthal angle for the baseline model is shown with the location of the indicated blade (IB) illustrated in the contours and this angle for the optimized model is defined and measured in plane II. Examining the vorticity contour plots indicates that the stream separation in the optimized model is greatly reduced compared to the baseline model, suggesting that the twisted and cambered blade will be effective in regulating the spraying vortices over blades by suppressing dynamic-stall. According to Figure 17, in the baseline model, dynamic-stall on the turbine blade increases as the angle of attack increases by turbine rotation. Significant stream separation is seen at azimuthal angle of 45^o and this is expanded until azimuthal angle of 90^o. On the other hand, the optimized turbine which takes advantage of twisted and cambered blades, can suppress dynamic-stall by interacting with water in a different angle of attack at each azimuthal angle. In the baseline model, which has straight-blades, the turbine interacts with water with constant angle of attack; however, twisted blades interact with water with different angles of attack at different points on the blade. To illustrate this effect, in Figure 17 all contours are plotted in three different planes. For instance, at azimuthal angle of 45^o (plane I) of the optimized model, the separation is almost negligible in comparison with the same plane for the baseline model. This can be explained by considering the moment coefficient (C_t) and pressure coefficient (Q_p) curves of both turbines. According to Figure 15, the average moment coefficient of the optimized turbine is 30% higher than the baseline one from azimuthal angles of 45^o to 90^o. Moreover, based on Figure 16, the torque that the positive cambered blade generates is consistently higher than the torque produced by the symmetric blade (baseline) due to greater lifting force. In addition, the wake (the span labelled "W" in Figure 17) generated by the baseline model stretches to a large region of the turbine blade, while for the optimized turbine it is a smaller region. The maximum region of wake for the baseline model is between 45^o to 90^o. In all contours plots displayed in the 4 azimuthal angles, the span of produced wake in the baseline model is more than the optimized one, which results in decrease in kinetic energy and in effect, lowers the performance of the turbine.

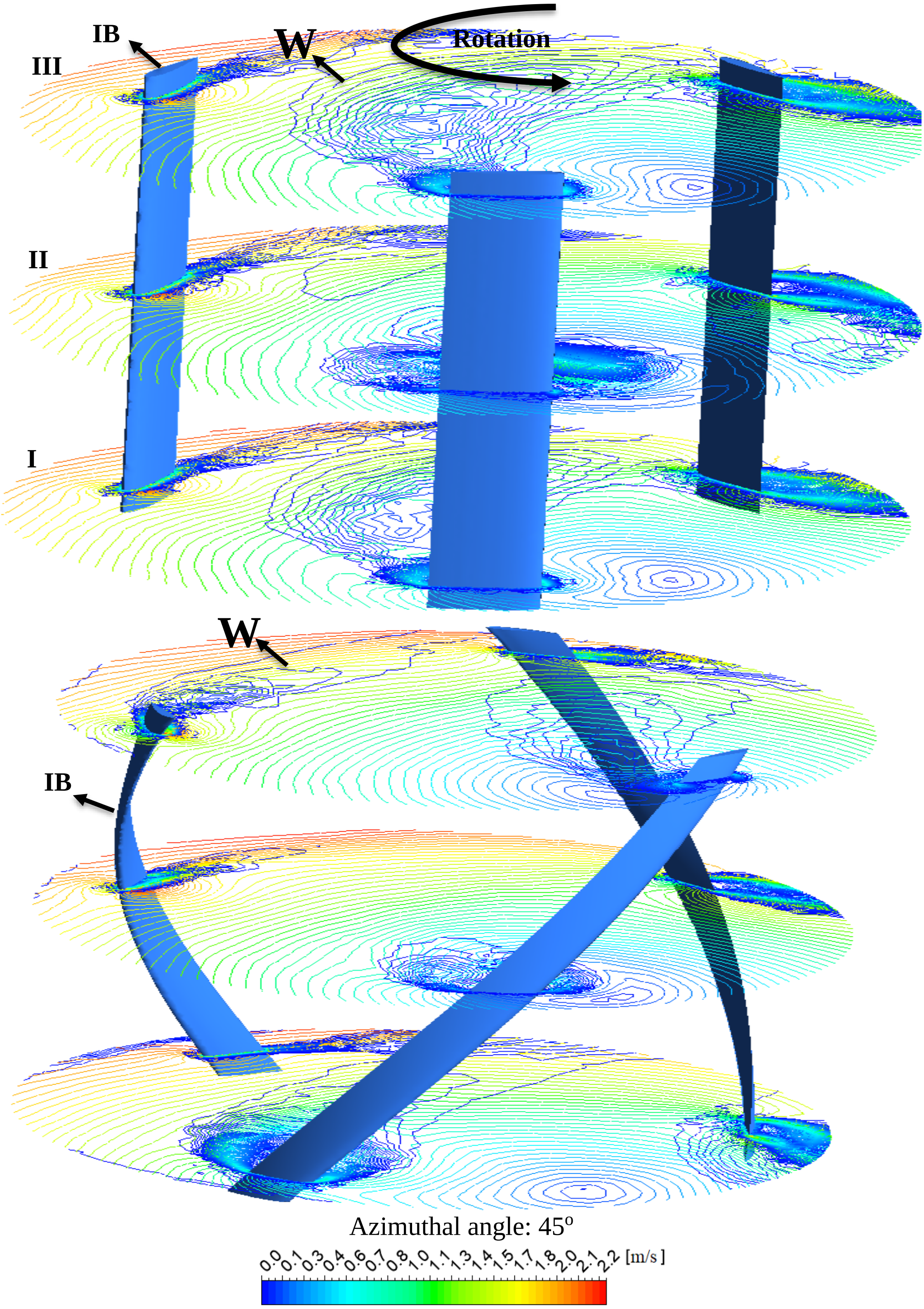
IB
III
W
Rotation
II
I
W
IB
Azimuthal angle: 45°
0.0 0.1 0.3 0.4 0.6 0.7 0.8 1.0 1.1 1.3 1.4 1.5 1.7 1.8 2.0 2.1 2.2 [m/s]

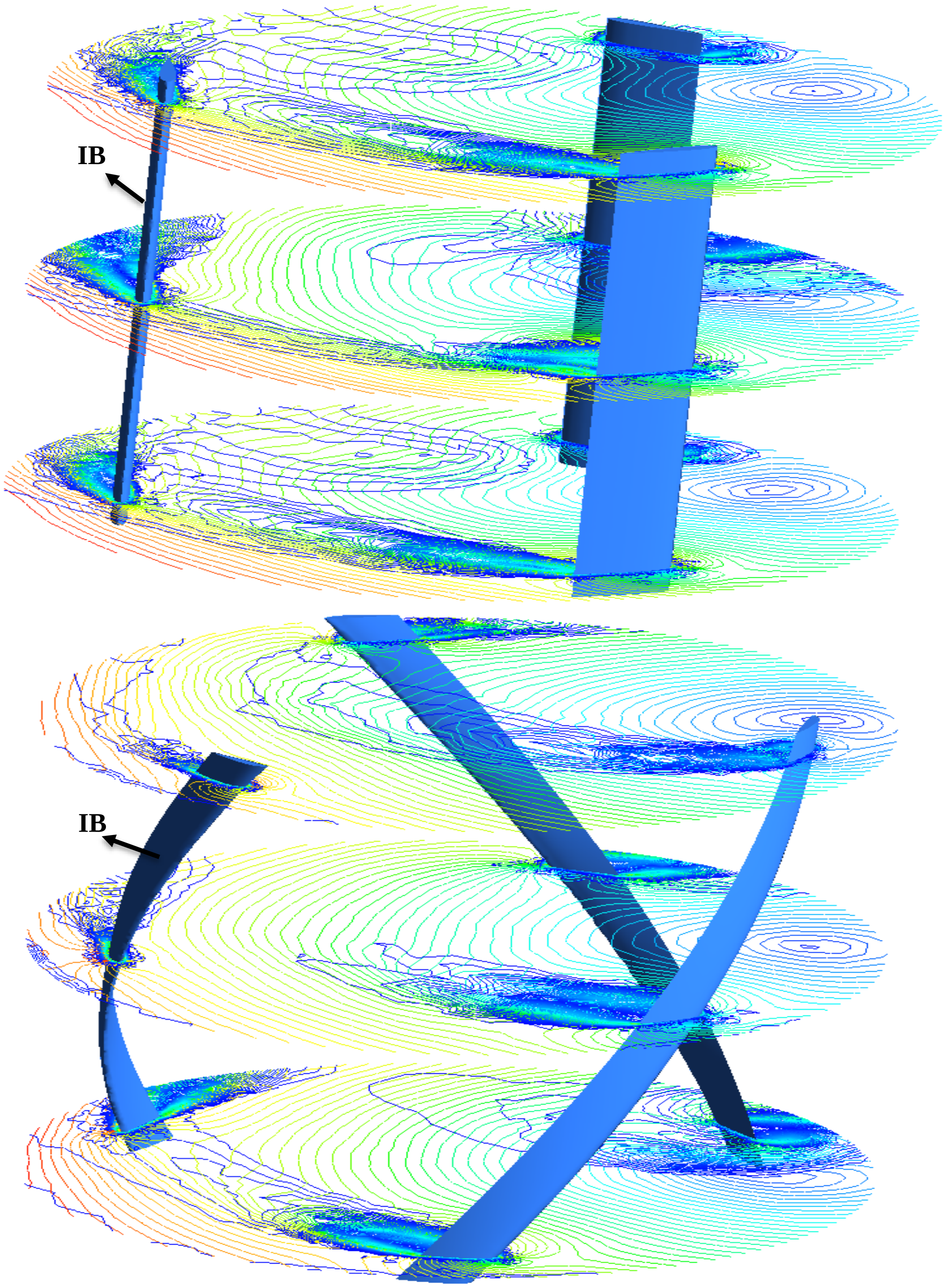

Azimuthal angle: 90°

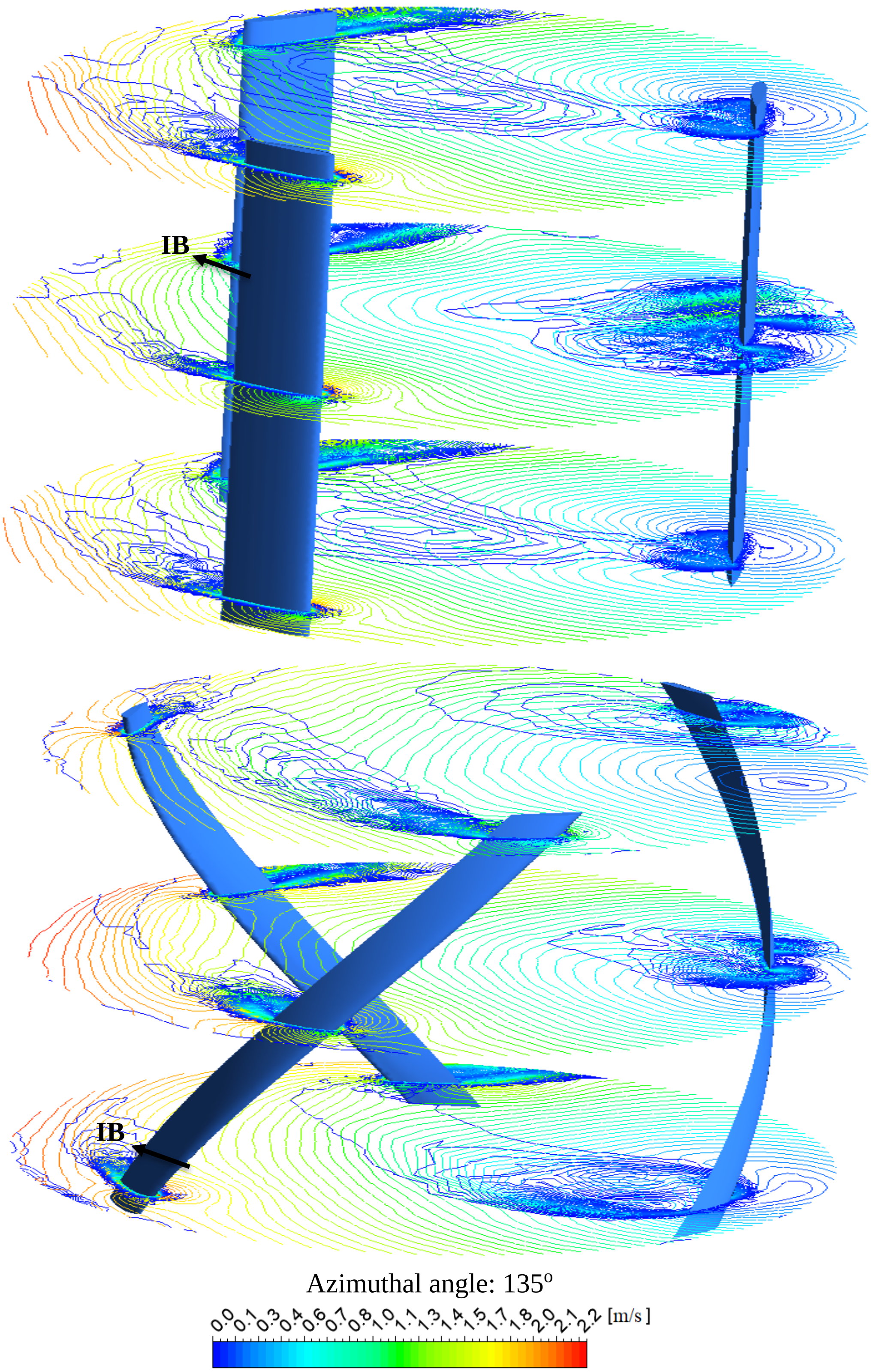
IB
IB
Azimuthal angle: 135°
0.0 0.1 0.3 0.4 0.6 0.7 0.8 1.0 1.1 1.3 1.4 1.5 1.7 1.8 2.0 2.1 2.2 [m/s]

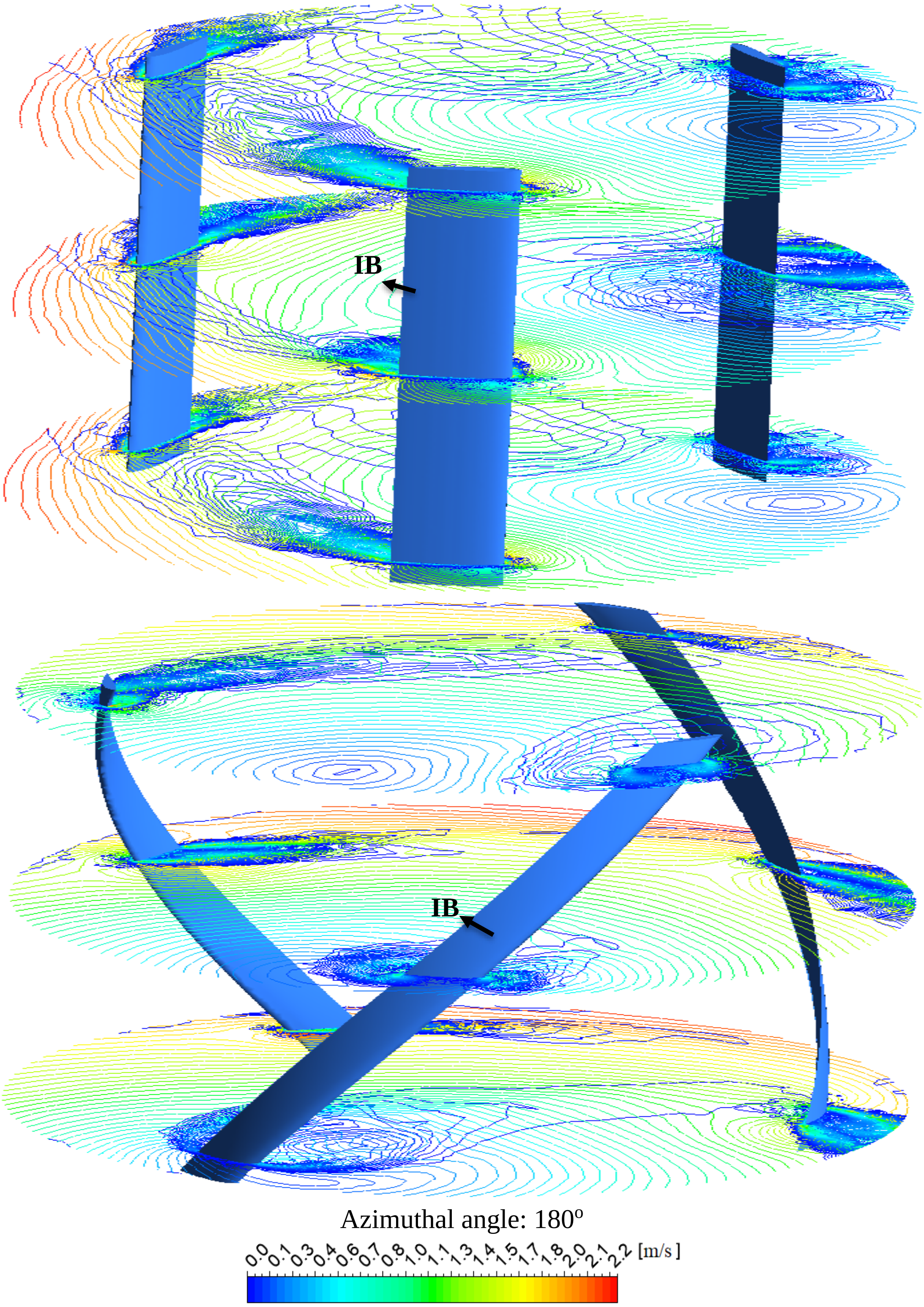

Figure 17. Vorticity distribution for the baseline and optimized models on 3 different planes.

5. Conclusion

In this research, a mixed-level Taguchi approach and comprehensive CFD simulations were employed to optimize the main parametric factors that affect the hydrodynamic performance of a VAT turbine. The following conclusions can be drawn from the results presented in this paper:

(1) The highest average moment coefficient (C_t) and power coefficient (C_p) correspond to case 12 which are 0.134 and 0.202 respectively. The value of C_p (0.202) obtained for case 12 is 21% higher than the baseline case (0.16). The S/N ratios of the 18 different cases were calculated. The maximum S/N ratio occurred at the maximum power coefficient. The maximum S/N ratio is 8.232 which corresponds to case 12.

(2) The results of the Taguchi method show that the combination of A_4, B_3, C_2, and D_2 results in the maximum output. The values of θ for factors A, B, C, and D are 0.863, 0.136, 0.151, and 0.684 respectively. This implies that twist angle is the most significant factor among the 4 tested factors, affecting the hydrodynamic performance of the turbine.

(3) Superposition method was used to estimate all possible responses (S/N ratios) outside orthogonal array (OA). The results of the superposition method showed that case 104 has the highest S/N ratio which is higher than the optimal design obtained by the Taguchi method (case 12). The value of S/N ratio for case 104 is 13% higher than case 12.

(4) The power coefficient (C_p) of the optimized turbine was calculated as 0.210, which is 24% higher than the baseline case. In addition, the optimized model reduced the required material by 57% compared with the baseline model, indicating that the new model is more economical. Moreover, the size of the wake generated in the baseline model was greater than the optimized model, resulting in a decrease in kinetic energy and a reduction in turbine output.

In this paper, the effects of vibration and deformation of turbine blades have not been considered. The interaction between water and structure and turbine frame is another factor that was not taken into consideration. Moreover, the blade roughness which is caused by erosion or/and dogged marine animals, affects the hydrodynamic performance and can be considered as a factor in the Taguchi method and its individual impacts as well as combination with other factors can be investigated.

Declaration of Competing Interest

The authors declare that they have no known competing financial interests or personal relationships that could have appeared to influence the work reported in this paper.

Acknowledgement

The authors would like to acknowledge the financial support from the College of Engineering, Mathematics and Physical Sciences of the University of Exeter for this project.

References

1. Finnegan, W., et al., *Operational fatigue loading on tidal turbine blades using computational fluid dynamics.* Renewable Energy, 2020. **152**: p. 430-440.
2. Abuan, B.E. and R.J. Howell, *The performance and hydrodynamics in unsteady flow of a horizontal axis tidal turbine.* Renewable Energy, 2019. **133**: p. 1338-1351.
3. Zhu, F.-w., et al., *Blade design and optimization of a horizontal axis tidal turbine.* Ocean Engineering, 2020. **195**: p. 106652.
4. Khanjanpour, M., A. Javadi, and M. Akrami, *CFD analyses of a tidal hydro-turbine (THT) for utilising in sea water desalination.* In Proceedings of the ISER 209th International Conference, London, UK, 7 July, 2019.
5. Ling, C., et al., *Economic evaluation of reverse osmosis desalination system coupled with tidal energy.* Frontiers in Energy, 2018. **12**(2): p. 297-304.
6. Baratchi, F., T. Jeans, and A.G. Gerber, *A modified implementation of actuator line method for simulating ducted tidal turbines.* Ocean Engineering, 2019. **193**: p. 106586.
7. Ahmadi, M.H. and Z. Yang, *The evolution of turbulence characteristics in the wake of a horizontal axis tidal stream turbine.* Renewable Energy, 2019.
8. Bouhal, T., et al., *CFD performance enhancement of a low cut-in speed current Vertical Tidal Turbine through the nested hybridization of Savonius and Darrieus.* Energy conversion and management, 2018. **169**: p. 266-278.
9. Zhang, X.-w., et al., *Research on the unsteady hydrodynamic characteristics of vertical axis tidal turbine.* China ocean engineering, 2014. **28**(1): p. 95-103.
10. Kumar, P.M., et al., *Multi-fidelity optimization of blade thickness parameters for a horizontal axis tidal stream turbine.* Renewable energy, 2019. **135**: p. 277-287.

11. Khanjanpour, M.H. and A. A. Javadi, *Experimental and CFD Analysis of Impact of Surface Roughness on Hydrodynamic Performance of a Darrieus Hydro (DH) Turbine.* energies, 2020.
12. Pongduang, S., C. Kayankannavee, and Y. Tiaple, *Experimental investigation of helical tidal turbine characteristics with different twists.* Energy Procedia, 2015. **79**: p. 409-414.
13. Zhang, T., et al., *A numerical study on choosing the best configuration of the blade for vertical axis wind turbines.* Journal of Wind Engineering and Industrial Aerodynamics, 2020. **201**: p. 104162.
14. Heavey, S.C., S.B. Leen, and J.P. McGarry, *Hydrodynamic Design and Analysis of a Novel Vertical Axis Turbine.* International Journal of Offshore and Polar Engineering, 2018. **28**(04): p. 393-401.
15. Hong, Y.-Y., A.A. Beltran Jr, and A.C. Paglinawan, *A robust design of maximum power point tracking using Taguchi method for stand-alone PV system.* Applied energy, 2018. **211**: p. 50-63.
16. Jahanshahi, M., M. Sanati, and Z. Babaei, *Optimization of parameters for the fabrication of gelatin nanoparticles by the Taguchi robust design method.* Journal of Applied Statistics, 2008. **35**(12): p. 1345-1353.
17. Wang, S. and G.H. Huang, *A multi-level Taguchi-factorial two-stage stochastic programming approach for characterization of parameter uncertainties and their interactions: An application to water resources management.* European Journal of Operational Research, 2015. **240**(2): p. 572-581.
18. Sapakal[1], S. and M. Telsang, *Parametric optimization of MIG welding using Taguchi design method.* Int J Adv Eng Res Stud, 2012. **1**(4): p. 28-30.
19. Chan, L.C., et al., *Optimisation of a conceptual aircraft model using a genetic algorithm and 3D Computational Fluid Dynamics (CFD).* 2019.
20. Rao, S.S. *Robust Design of Horizontal Axis Wind Turbines Using Taguchi Method*. in *ASME 2015 International Mechanical Engineering Congress and Exposition*. 2015. American Society of Mechanical Engineers Digital Collection.
21. Wang, Z., Y. Wang, and M. Zhuang, *Improvement of the aerodynamic performance of vertical axis wind turbines with leading-edge serrations and helical blades using CFD and Taguchi method.* Energy conversion and management, 2018. **177**: p. 107-121.
22. Permanasari, A.A., et al. *Experimental Investigation and Optimization of Floating Blade Water Wheel Turbine Performance Using Taguchi Method and Analysis of Variance (ANOVA)*. in *IOP Conference Series: Materials Science and Engineering*. 2019. IOP Publishing.
23. Nandagopal, R.A. and S. Narasimalu, *Multi-objective optimization of hydrofoil geometry used in horizontal axis tidal turbine blade designed for operation in tropical conditions of South East Asia.* Renewable Energy, 2020. **146**: p. 166-180.
24. Ma, Y., et al., *Optimization of blade motion of vertical axis turbine.* China Ocean Engineering, 2016. **30**(2): p. 297-308.
25. Alidadi, M., *Duct optimization for a ducted vertical axis hydro current turbine*. 2009, University of British Columbia.
26. Hwang, I.S., Y.H. Lee, and S.J. Kim, *Optimization of cycloidal water turbine and the performance improvement by individual blade control.* Applied Energy, 2009. **86**(9): p. 1532-1540.
27. Mannion, B., S.B. Leen, and S. Nash, *Development and assessment of a blade element momentum theory model for high solidity vertical axis tidal turbines.* Ocean Engineering, 2020. **197**: p. 106918.

28. Luo, Q.-J., et al. *Optimization of blade deflection angle of vertical-axis turbine for tidal current energy conversion*. in *The Twentieth International Offshore and Polar Engineering Conference*. 2010. International Society of Offshore and Polar Engineers.
29. Batten, W., et al., *Experimentally validated numerical method for the hydrodynamic design of horizontal axis tidal turbines.* Ocean engineering, 2007. **34**(7): p. 1013-1020.
30. Tunio, I.A., et al., *Investigation of duct augmented system effect on the overall performance of straight blade Darrieus hydrokinetic turbine.* Renewable Energy, 2020. **153**: p. 143-154.
31. Ai, K., et al., *Numerical modelling of a dual-rotor marine current turbine in a rectilinear tidal flow.* Ocean Engineering, 2020. **200**: p. 107026.
32. Kundu, P., *Numerical simulation of the effects of passive flow control techniques on hydrodynamic performance improvement of the hydrofoil.* Ocean Engineering, 2020. **202**: p. 107108.
33. Asr, M.T., et al., *Study on start-up characteristics of H-Darrieus vertical axis wind turbines comprising NACA 4-digit series blade airfoils.* Energy, 2016. **112**: p. 528-537.
34. Kishore, R., C. Stewart, and S. Priya, *Wind Energy Harvesting: Micro-to-small Scale Turbines*. 2018: Walter de Gruyter GmbH & Co KG.
35. Nabavi, Y., *Numerical study of the duct shape effect on the performance of a ducted vertical axis tidal turbine*. 2008, University of British Columbia.
36. Laín Beatove, S. and C. Osorio, *Simulation and evaluation of a straight-bladed Darrieus-type cross flow marine turbine.* 2010.
37. Yang, W., Y. Wu, and S. Liu, *An optimization method on runner blades in bulb turbine based on CFD analysis.* Science China Technological Sciences, 2011. **54**(2): p. 338-344.
38. Chowdhury, A.M., H. Akimoto, and Y. Hara, *Comparative CFD analysis of Vertical Axis Wind Turbine in upright and tilted configuration.* Renewable energy, 2016. **85**: p. 327-337.
39. Liu, Z., H. Qu, and H. Shi, *Numerical Study on Self-Starting Performance of Darrieus Vertical Axis Turbine for Tidal Stream Energy Conversion.* Energies, 2016. **9**(10): p. 789.
40. Badshah, M., S. Badshah, and S. Jan, *Comparison of computational fluid dynamics and fluid structure interaction models for the performance prediction of tidal current turbines.* Journal of Ocean Engineering and Science, 2019.
41. Asghar, U., I. Aziz, and F. Sher. *Modelling and simulation of flow induced vibrations in vertical axis wind turbine blade*. in *2017 14th International Bhurban Conference on Applied Sciences and Technology (IBCAST)*. 2017. IEEE.
42. De Lellis, M., et al., *The Betz limit applied to airborne wind energy.* Renewable Energy, 2018. **127**: p. 32-40.
43. Chen, W.-H., et al., *Power output analysis and optimization of two straight-bladed vertical-axis wind turbines.* Applied energy, 2017. **185**: p. 223-232.
44. Bao, Z., et al., *Optimal design of metal hydride reactors based on CFD–Taguchi combined method.* Energy Conversion and Management, 2013. **65**: p. 322-330.
45. Phadke, M.S., *Quality engineering using robust design*. 1995: Prentice Hall PTR.
46. Pasha, M., et al., *Effects of quality characteristic distributions on the integrated model of Taguchi's loss function and economic statistical design of-control charts by modifying the Banerjee and Rahim economic model.* Communications in Statistics-Theory and Methods, 2018. **47**(8): p. 1842-1855.

47. Vennell, R., *Exceeding the Betz limit with tidal turbines.* Renewable Energy, 2013. **55**: p. 277-285.
48. Petit, H.A., et al., *Modelling and optimization of an inclined plane classifier using CFD-DPM and the Taguchi method.* Applied Mathematical Modelling, 2020. **77**: p. 617-634.
49. Mandal, N., et al., *Optimization of flank wear using Zirconia Toughened Alumina (ZTA) cutting tool: Taguchi method and Regression analysis.* Measurement, 2011. **44**(10): p. 2149-2155.
50. Freddi, A. and M. Salmon, *Introduction to the Taguchi method*, in *Design Principles and Methodologies*. 2019, Springer. p. 159-180.
51. Nicholls-Lee, R., S. Turnock, and S. Boyd, *Performance prediction of a free stream tidal turbine with composite bend-twist coupled blades.* 2008.
52. Danao, L.A., N. Qin, and R. Howell, *A numerical study of blade thickness and camber effects on vertical axis wind turbines.* Proceedings of the Institution of Mechanical Engineers, Part A: Journal of Power and Energy, 2012. **226**(7): p. 867-881.
53. Naoi, K., et al. *A Wind Power Generation System using the Vertical Axis Wind Turbine with Arc Camber Blades*. in *The Sixteenth International Offshore and Polar Engineering Conference*. 2006. International Society of Offshore and Polar Engineers.
54. Ouro, P., T. Stoesser, and L. Ramírez, *Effect of blade cambering on dynamic stall in view of designing vertical axis turbines.* Journal of Fluids Engineering, 2018. **140**(6).
55. Sutikno, P., et al. *Experimental of Three Parallel Water Current Turbine with Optimized Straight Blades and Using Flow Concentrator Channeling Device to Augmented Performance and Self-Starting Capability*. in *Applied Mechanics and Materials*. 2015. Trans Tech Publ.
56. Urbina, R., et al., *A dynamic stall model for analysis of cross-flow turbines using discrete vortex methods.* Renewable energy, 2019. **130**: p. 1130-1145.
57. Gupta, R. and A. Biswas, *Computational fluid dynamics analysis of a twisted three-bladed H-Darrieus rotor.* Journal of Renewable and Sustainable Energy, 2010. **2**(4): p. 043111.
58. Dai, Y. and W. Lam, *Numerical study of straight-bladed Darrieus-type tidal turbine.* Proceedings of the Institution of Civil Engineers-Energy, 2009. **162**(2): p. 67-76.
59. Mohan Kumar, P., et al., *Strategies for Enhancing the Low Wind Speed Performance of H-Darrieus Wind Turbine—Part 1.* Clean Technologies, 2019. **2**(1): p. 32-51.
60. Paraschivoiu, I., *Wind turbine design: with emphasis on Darrieus concept*. 2002: Presses inter Polytechnique.
61. Brusca, S., R. Lanzafame, and M. Messina, *Design of a vertical-axis wind turbine: how the aspect ratio affects the turbine's performance.* International Journal of Energy and Environmental Engineering, 2014. **5**(4): p. 333-340.
62. Armstrong, S., A. Fiedler, and S. Tullis, *Flow separation on a high Reynolds number, high solidity vertical axis wind turbine with straight and canted blades and canted blades with fences.* Renewable Energy, 2012. **41**: p. 13-22.
63. Hasçalık, A. and U. Çaydaş, *Optimization of turning parameters for surface roughness and tool life based on the Taguchi method.* The International Journal of Advanced Manufacturing Technology, 2008. **38**(9-10): p. 896-903.
64. Roy, R.K., *A primer on the Taguchi method*. 2010: Society of Manufacturing Engineers.
65. Naik, A.B. and A.C. Reddy, *Optimization of tensile strength in TIG welding using the Taguchi method and analysis of variance (ANOVA).* Thermal Science and Engineering Progress, 2018. **8**: p. 327-339.

66. Ranganath, M. and R. Vipin, *Optimization of Process Parameters in Turning Operation of Aluminium (6061) with Cemented Carbide Inserts Using Taguchi Method and Anova.* International Journal, 2013. **1**(1): p. 13-21.
67. Ott, R.L. and M.T. Longnecker*, An introduction to statistical methods and data analysis*. 2015: Nelson Education.
68. Abuthakeer, S., P. Mohanram, and G.M. Kumar, *Prediction and control of cutting Tool vibration in CNC Lathe with ANOVA and ANN.* International Journal of Lean Thinking, 2011. **2**(1): p. 1-23.
69. Ma, L., et al., *Dynamic Stall of a Vertical-Axis Wind Turbine and Its Control Using Plasma Actuation.* Energies, 2019. **12**(19): p. 3738.
70. Chen, Y. and Y. Lian, *Numerical investigation of vortex dynamics in an H-rotor vertical axis wind turbine.* Engineering Applications of Computational Fluid Mechanics, 2015. **9**(1): p. 21-32.
71. Walker, J.M., et al., *Experimental and numerical studies of blade roughness and fouling on marine current turbine performance.* Renewable Energy, 2014. **66**: p. 257-267.
72. Li, S., et al., *Design and testing of a LUT airfoil for straight-bladed vertical axis wind turbines.* Applied Sciences, 2018. **8**(11): p. 2266.
73. Jawahar, H.K., et al., *Aerodynamic and aeroacoustic performance of high-lift airfoil fitted with slat cove fillers.* Journal of Sound and Vibration, 2020: p. 115347.